PAPER

Arterial pressure pulse wave separation analysis using a multi-Gaussian decomposition model

IOP Publishing Physiol. Meas. 43 (2022) 055005 https://doi.org/10.1088/1361-6579/ac6e56

Physiological Measurement

IPEM Institute of Physics and Engineering in Medicine

RECEIVED
13 December 2021

REVISED
5 May 2022

ACCEPTED FOR PUBLICATION
10 May 2022

PUBLISHED
31 May 2022

PAPER

Arterial pressure pulse wave separation analysis using a multi-Gaussian decomposition model

Rahul Manoj[1], **Kiran V Raj**[1], **P M Nabeel**[2], **Mohanasankar Sivaprakasam**[1,2] **and Jayaraj Joseph**[1]

[1] Department of Electrical Engineering, Indian Institute of Technology Madras, Chennai, India
[2] Healthcare Technology Innovation Centre, Indian Institute of Technology Madras, Chennai, India

E-mail: rahul_manoj@smail.iitm.ac.in

Keywords: wave separation analysis, wave intensity analysis, pulse wave reflection, reflection magnitude, reflection index, multi-Gaussian, modelling of pulse wave

Abstract

Objective. Methods for separating the forward–backward components from blood pulse waves rely on simultaneously measured pressure and flow velocity from a target artery site. Modelling approaches for flow velocity simplify the wave separation analysis (WSA), providing a methodological and instrumentational advantage over the former; however, current methods are limited to the aortic site. In this work, a multi-Gaussian decomposition (MGD) modelled WSA (MGD_{WSA}) is developed for a non-aortic site such as the carotid artery. While the model is an adaptation of the existing wave separation theory, it does not rely on the information of measured or modelled flow velocity. *Approach.* The proposed model decomposes the arterial pressure waveform using weighted and shifted multi-Gaussians, which are then uniquely combined to yield the forward ($P_F(t)$) and backward ($P_B(t)$) pressure wave. A study using the database of healthy (virtual) subjects was used to evaluate the performance of MGD_{WSA} at the carotid artery and was compared against reference flow-based WSA methods. *Main results.* The MGD modelled pressure waveform yielded a root-mean-square error (RMSE) < 0.35 mmHg. Reliable forward–backward components with a group average RMSE <2.5 mmHg for $P_F(t)$ and $P_B(t)$ were obtained. When compared with the reference counterparts, the pulse pressures (ΔP_F and ΔP_B), as well as reflection quantification indices, showed a statistically significant strong correlation ($r > 0.96, p < 0.0001$) and ($r > 0.83, p < 0.0001$) respectively, with an insignificant ($p > 0.05$) bias. *Significance.* This study reports WSA for carotid pressure waveforms without assumptions on flow conditions. The proposed method has the potential to adapt and widen the vascular health assessment techniques incorporating pulse wave dynamics.

1. Introduction

The pressure pulse comprises a forward and backward propagating wave at any given arterial site. The forward component of the pressure wave originates from the left ventricular ejection. It travels from the aortic root to peripheral arterial sites, while the backward component travels back to the heart from various reflection sites across the arterial bed (Mynard *et al* 2020). The changes in the characteristic impedance of the blood vessels, due in part to the vessel geometry changes (tapering or branching), vessels' stiffness gradient, or impedance of peripheral sites (Westerhof and Westerhof 2012), are potential reflection sites (Segers *et al* 2017). The rhythmic addition of forward and backward (reflected) waves forms the final pressure wave, which plays a vital role in maintaining the pulsatile-steady blood flow equilibrium between the elastic-muscular arteries and end-organ micro-circulation (Nichols *et al* 2011). The magnitude and timing of reflected wave on final pressure pulse derange when an arterial tree is exposed to cardiovascular risk factor(s) and ageing (London *et al* 2019). An early return of the reflected waves will raise the central arterial pulse pressure, increasing the cardiac load and boosting the systolic pressure, which has proven to cause fatal and non-fatal cardiovascular events (Haider *et al* 2003,

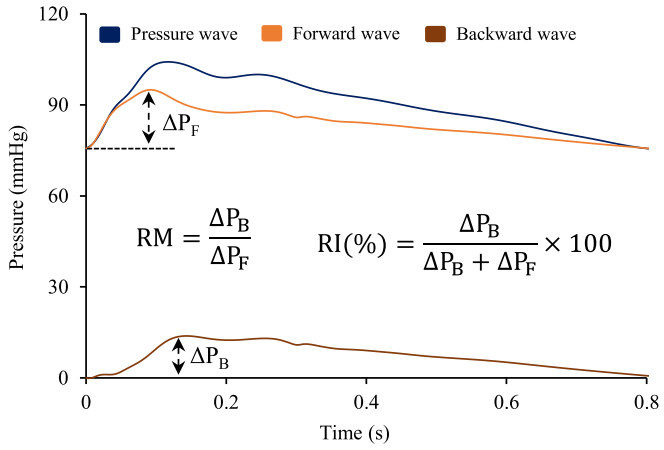

Figure 1. The pressure waveform is separated into its forward and backward components with mathematical expressions for reflection quantification indices (RM and RI).

Tomiyama *et al* 2013). Therefore, the analysis and quantification of the phenomenon of pulse wave reflection in the arterial tree have been of increasing interest in the clinical and research community for several years now.

Among the methods proposed to quantify reflection, the Augmentation Index (AIx) is currently being widely used (Wilkinson *et al* 1998, Papaioannou *et al* 2004). However, the factors such as the identification of pulses' inflection (or shoulder) point, the height of the subject, arterial stiffness gradient, and confounding effect of the heart rate, challenge the reliability of AIx (Segers *et al* 2009, Hughes *et al* 2013). Thus, its role in quantifying the reflection component is debated (Segers *et al* 2007). On the other hand, a more reliable method to quantify reflection is based on pulse wave separation analysis (WSA) (Swillens and Segers 2008). An accurate WSA technique relies on the morphology of simultaneously measured (ideally from a single site) arterial pressure and blood flow velocity waves. Implementation of such WSA has been performed either in the frequency domain (FD_{WSA}) (Westerhof *et al* 1972) or time-domain (TD_{WSA}) (Jones and Parker 1990). Both the approaches have proven to be comparable in quantifying the reflection phenomenon in terms of Reflection Magnitude (RM) and Reflection Index (RI) (van den Wijngaard *et al* 2009, Westerhof *et al* 2015). As depicted in figure 1, RM is the ratio between the pulse pressure of a backward wave (ΔP_B) to that of a forward wave (ΔP_F), and RI is the ratio of ΔP_B expressed as a percentage of the total pulse pressure of forward and backward waves ($\Delta P_F + \Delta P_B$). Similar to RM and RI; the reflection wave transit time (RWTT) provides information on pulse wave reflection as the transit time between forward and backward wave (Segers *et al* 2007, Qasem and Avolio 2008). It is important to note that the synchronized, simultaneous acquisition of reliable pressure and flow velocity from an arterial site has its practical challenges (Hoeks *et al* 2000). Subsequently, simplified WSA techniques have been proposed by modelling required flow velocity waveforms from the measured pressure wave (Westerhof *et al* 2006, Kips *et al* 2009, Swamy *et al* 2010, Hametner *et al* 2013).

One popular approach in modelling flow velocity for WSA is the triangular approximation of the aortic flow velocity (TF_{WSA}) wave (Westerhof *et al* 2006), wherein the peak and base of the flow velocity-triangle are identified based on the pulse wave inflection point and the ejection period of the heart, respectively. Another prominent work reports a method to obtain an average flow velocity waveform from a subset (say 3%) of the total study population (Kips *et al* 2009). While this approach provides an alternative and physiologically more accurate solution for aortic flow velocity modelling, the need for the measured flow velocity information from at least a subset of the target cohort is a practical concern. A modified three-element Windkessel based model for aortic flow velocity has shown performance comparable to average flow velocity and better than the triangular flow velocity model (Hametner *et al* 2013). The forward–backward pulse wave separation based on the arterial tube-load model (Swamy *et al* 2010) assumes the (small) peripheral arteries as the dominant reflection sites while neglecting the magnitude of reflection caused by the branching and tapering of large arteries. It is noteworthy that aforesaid models are proposed for approximating the central aortic blood flow velocity for WSA (Mynard *et al* 2020). Further, their applicability and validation in literature have also been limited to aortic flow velocity.

We propose a multi-Gaussian decomposition (MGD) modelled WSA for large arteries such as the carotid artery, using pressure pulse waves. The method's performance was demonstrated on the common carotid artery, a site that is superficial, easily accessible for non-invasive measurements, and closely represents the aortic conditions (Laurent *et al* 2006). It is worth noting, that such carotid wave separation and reflection analysis have been recently demonstrated advantageous for several clinical applications (Zambanini *et al* 2005, Chiesa *et al* 2019). Mathematical modelling of MGD modelled WSA (MGD_{WSA}), and its implementation methodology are

discussed in the following section. A study using the database of 4374 healthy virtual subjects (Charlton *et al* 2019) was performed to (i) evaluate the feasibility of the MGD_{WSA} in separating the forward and backward components of the carotid pressure waveform, (ii) evaluate the performance of the proposed method by comparing its forward–backward waves against those obtained from the state-of-the-art WSA methods (TD_{WSA} and FD_{WSA}) and, (iii) compare the agreement of RM, RI and RWTT estimated using MGD_{WSA} with those derived from the state-of-the-art WSA methods. The study results and observations are discussed, accompanying insights to allied future research.

2. Materials and methods

The theory of MGD_{WSA} is detailed in this section, followed by a description of the study population, data processing and analysis employed. The study initially focuses on a parametric analysis to understand the influence of the model parameters on the accuracy of the reflection quantification indices (RM, RI, RWTT, ΔP_B, and ΔP_F). Post arriving at a recommended optimal design parameter for MGD_{WSA}, its performance was evaluated against the state-of-the-art WSA methods using pressure and flow velocity. The performance evaluation of the proposed model aims to assess the accuracy of MGD modelled pressure wave, separated forward–backward waves, and the agreement of reflection quantification indices such as RM RI and RWTT derived from the proposed model. The comparison was performed against the indices derived from (i) WSA in the frequency domain (FD_{WSA}) (Westerhof *et al* 1972), and (ii) WSA in the time domain (TD_{WSA}) (Jones and Parker 1990).

2.1. Mathematical modelling

The wave separation theory derived from the electrical transmission line circuit analogy (Westerhof *et al* 1972) expresses the forward ($P_F(t)$) and backward ($P_B(t)$) components of an arterial pressure $P(t)$ as:

$$P_F(t) = \frac{1}{2}(P(t) + U(t) \times Z_c) \tag{1}$$

and,

$$P_B(t) = \frac{1}{2}(P(t) - U(t) \times Z_c), \tag{2}$$

where $U(t)$ is blood flow velocity and Z_C is the magnitude of the characteristic impedance of the target blood vessel (Qureshi *et al* 2018). When $P(t)$ is represented as a sum of two functions, say $F_1(t)$ and $F_2(t)$, it gives:

$$P(t) = F_1(t) + F_2(t) \tag{3}$$

such that,

$$F_1(t) = U(t) \times Z_c \tag{4}$$

and

$$F_2(t) = P(t) - (U(t) \times Z_c). \tag{5}$$

By substituting (4) and (5) in (1) and (2), an expression for $P_F(t)$ and $P_B(t)$ can be written as:

$$P_B(t) = \frac{F_2(t)}{2} \tag{6}$$

and

$$P_F(t) = F_1(t) + \frac{F_2(t)}{2}. \tag{7}$$

The proposed MGD_{WSA} decomposes $P(t)$ to a set of weighted and shifted Gaussians, which are then uniquely combined to yield two functions $G_1(t)$ and $G_2(t)$, equivalent to $F_1(t)$ and $F_2(t)$. Literature reports Gaussian functions as a rational wavelet choice to reliably construct an arterial pulse wave (Wang *et al* 2013). Of the '*N*' Gaussians that decompose the pressure waveform, $G_1(t)$ is obtained from the first '*n*' among the Gaussians (when sorted by the ascending order of time-positions) that exist till the dicrotic notch of $P(t)$. Further, $G_2(t)$ is constructed from the remaining 'N - n' Gaussians as,

$$G_1(t) = \sum_{i=1}^{n} g_i(t) \tag{8}$$

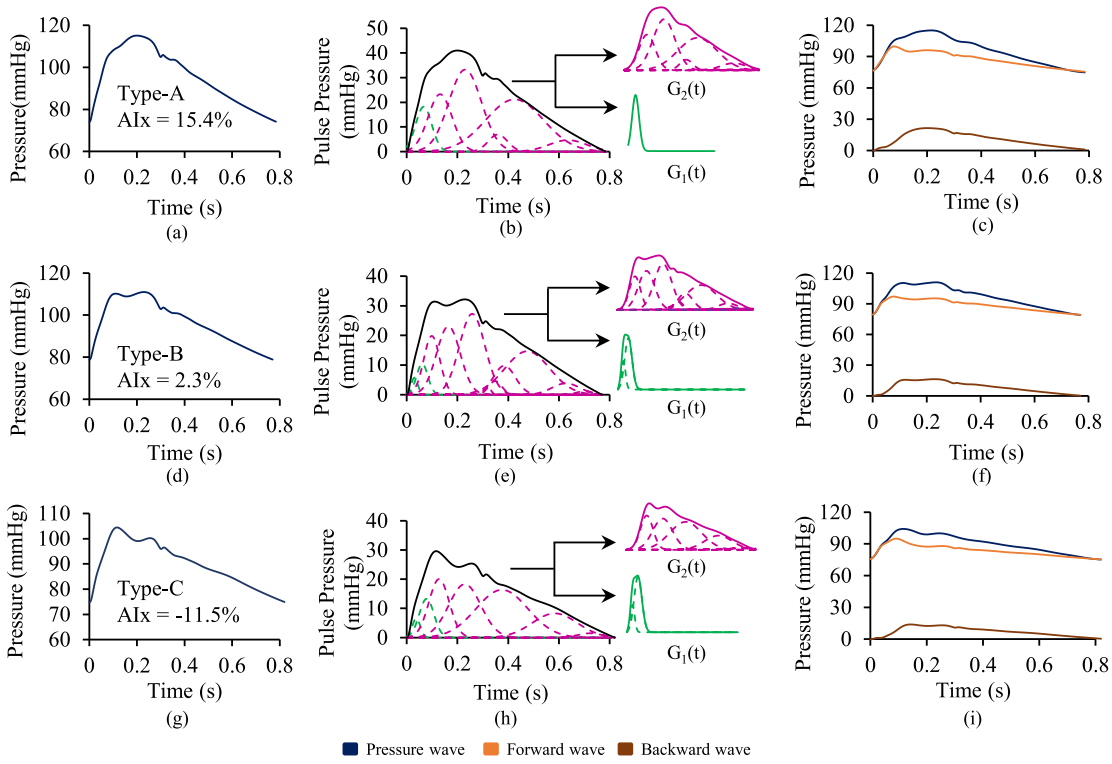

Figure 2. Wave separation using multi-Gaussian decomposition model for each type of the waveform morphology, (a)–(c) is Type-A, (d)–(f) is Type-B and (g)–(i) is for Type-C.

and

$$G_2(t) = \sum_{i=n+1}^{N} g_i(t), \tag{9}$$

where,

$$g_i(t) = A_i e^{-\frac{1}{2}\times\frac{(t-M_i)^2}{C_i^2}}. \tag{10}$$

In (10), A_i is the amplitude or weight, M_i is the mean locations, and C_i is the standard deviation from M_i for the respective Gaussian $g_i(t)$.

The decomposition of $P(t)$ is based on identifying the N Gaussians, the summation of which results in an approximated pressure waveform $\hat{P}(t;\ K)$. This $\hat{P}(t;\ K)$ is obtained by performing a nonlinear curve fit optimization using the Levenberg–Marquardt (LM) algorithm on $P(t)$. The LM algorithm optimizes the parameters ($K_i : A_i,\ M_i,\ C_i$) for a given N, by minimizing the weighted (W_j) sum of the squares of errors (χ^2) between ($\hat{P}(t;\ K)$) and $P(t)$ as,

$$\chi^2 = \sum W_j(P(j) - \hat{P}(j;\ K))^2 = \sum W_j\left(P(j) - \sum_{i=1}^{N} g_i(j)\right)^2. \tag{11}$$

Thus obtained Gaussians are used to construct $G_1(t)$ and $G_2(t)$ and hence, obtain $P_F(t)$ and $P_B(t)$ using (6) and (7), respectively. Wave decomposition using the MGD model and the forward–backward components for each Type of waveform morphology (Type-A, Type-B and Type-C (Takazawa *et al* 1995)) for a sample subject is illustrated in figure 2.

2.2. Data preparation

A database of 4374 healthy virtual subjects developed by the Hemodynamic Modelling Research Group of Kings College, London, UK, was used in this study. The database was created by computer simulations of the arterial tree's 1D numerical modelling (Alastruey *et al* 2012). A parametric input set obtained from literature on the variability of the cardiac, arterial, vascular bed and blood properties for an age group of 25–75 was used to create the pulse waves for each decade of the age group. The variations resulting from the above factors and the approach used to simulate pulse waves at different ages, validated against *in vivo* data, were reported (Charlton *et al* 2019).

The pressure waveform (in mmHg) and flow velocity waveform (in m s^{-1}) of the common carotid artery for the 4374 study population were extracted from the database. It was divided with a 1:5 ratio, into the development cohort and validation cohort. The development cohort comprises 900 subjects distributed across age groups 25–75 years and has an equal proportion of Type-A, Type-B and Type-C waveform morphology (300 subjects for each Type). This cohort was used for parametric analysis to obtain the optimal design parameters (N, n) of the MGD model. The validation cohort comprising 3475 subjects was then used to evaluate the performance of MGD_{WSA} against the FD_{WSA} and TD_{WSA} methods.

2.3. Data processing

Arterial pressure and flow velocity waveform were sampled at 500 Hz. For maintaining uniformity across all the subjects, a cycle trimming was performed on the pressure cycles to ensure it was produced solely from the systolic phase foot to its end-diastolic phase foot. The corresponding trimming window was applied to the flow velocity waveform. Before further analysis, any pressure waveforms exhibiting a baseline wandering were corrected by employing a linear baseline estimator. The required derivative waveforms (Takazawa *et al* 1995) for the calculation of AIx and classification of pressure waveforms into Type-A, Type-B and Type-C, were computed using a Savitzky–Golay's filter of 4th order polynomial and 28 side points, ensuring a 3 dB cut-off in the frequency spectrum of derivatives to be at 12 Hz (He *et al* 2014). Automated processing of the MGD_{WSA} and state-of-the-art WSA methods were implemented using LabVIEW® (National Instruments, USA).

The processed waveforms were first screened based on the inclusion criteria for the development cohort. The inclusion criteria for the selection of subjects in the development cohort were made in such a way that the absolute errors in RM and RI values between TD_{WSA} and FD_{WSA} are arranged in increasing order, and the first 300 subjects, with age diversity for each Type of the waveform, were considered (where the best-case absolute error was achieved). Thus, the prepared set yielded a high level of agreement (absolute errors in RM < 0.06 and RI $< 6.5\%$, r-value > 0.95) for the RM and RI estimates between frequency versus time-domain WSA. A parametric analysis was performed for this cohort by iteratively varying (N, n) within fixed boundaries. The pressure waveforms were decomposed using the MGD model, based on the values of (N, n) in each iteration, to obtain the RM and RI. A subset of (N, n) from all combinations of (N, n) was obtained such that the deviations in the values of RM and RI obtained from MGD_{WSA} for the given (N, n) against those from reference WSA methods were smaller than a defined tolerance level. From this subset, the most repetitive (N, n) (mode value) for each type of waveform morphology was deemed as the recommended design solution for MGD_{WSA}. The model designed from these combinations of (N, n) were applied to the validation cohort for performance evaluation.

2.4. Statistical analysis

All results were presented as mean $\pm$ standard deviations. The accuracy of the modelled pressure waveform and that of the separated forward and backward waves were analyzed using RMSE and absolute error. Regression analysis was performed between reflection quantification indices (RM, RI, RWTT, ΔP_F, ΔP_B) obtained from MGD_{WSA} and other WSA methods. The correlation between reflection quantification indices was reported using Pearson's correlation coefficient (r) and statistical significance in p-value. The performance of methods was compared through Bland–Altman (BA) plots reported with bias and confidence interval (CI, as Bias $\pm$ 1.96 Standard Deviation). ANOVA compared the similarity among reflection quantification indices obtained from all the methods versus MGD_{WSA}. The level of significance of $\alpha = 0.05$ was used for all tests. A p-value < 0.05 confirmed a statistical significance.

3. Results

3.1. Evaluation of design parameters—*N* and *n*

Figure 3 shows the influence of N on the fitting accuracy of the MGD-modelled pressure waveform. The RMSE between MGD-modelled and the true pressure waveforms (obtained from the virtual subjects database (Charlton *et al* 2019)) decreased gradually as N increased from 1 to 20. For $N = 15$, the RMSE was ~0.04 mmHg with no significant reduction achieved for $N > 15$. From $N > 5$, the group average RMSE was less than 0.5 mmHg, and the maximum absolute error between MGD-modelled and true pressure waveforms was <4.43 mmHg (in the neighbourhood of dicrotic notch).

Since the improvement in RMSE was insignificant beyond $N > 15$, the extrema for N were set to 15 as it yielded acceptable model accuracy at the expense of minimal computational overhead. Subsequently, combinations with N bounded from 6 to 15 were chosen for further parametric analyses. Note that the function $G_1(t)$ was constructed using a subset of Gaussians (n) present within the diastolic foot to dicrotic notch period. For the present data, n varied within $1 < n \leqslant 4$ and hence fixed its range.

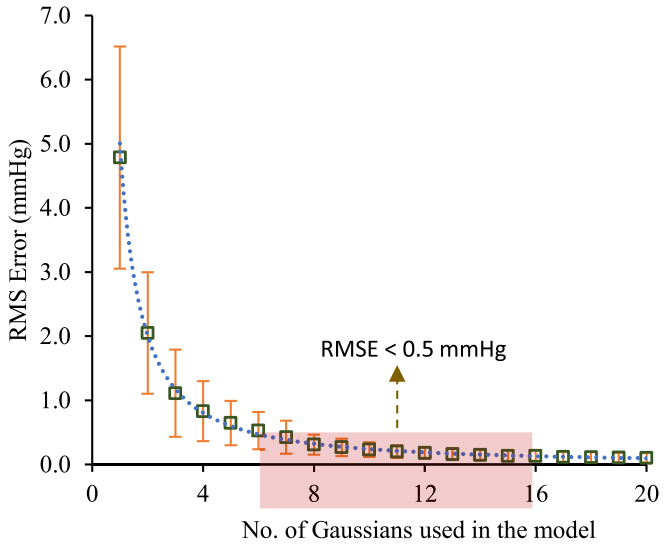

Figure 3. RMSE between true pressure waveform and MGD modelled pressure waveform by varying the number of Gaussians used for the nonlinear curve fitting algorithm.

From the potential combinations of (N: 6 $\rightarrow$ 15, n: 1 $\rightarrow$ 4), optimal subsets of (N, n) were obtained such that the deviation in RM and RI measures for each subject when compared against those derived from reference WSA methods fell within a tolerance level of 0.065% and 6.7%, respectively. (The tolerance level was defined based on the RMSE in RM and RI between the reference FD_{WSA} and TD_{WSA} methods for the entire population.) Therefore, these represent the ideal error boundaries for MGD_{WSA} when compared against both the references for the parametric analysis. Hence the analysis of MGD model yields an (N, n), such that the absolute error in RM and RI obtained from MGD_{WSA} is lesser than or equal to the values: 0.065 for RM and 6.7% for RI, when compared with either of the reference methods.

The heatmap in figure 4 illustrates the repetitive occurrence rate of (N, n) as a score out of 100% for each type of waveform morphology at a population level. The region in *Blue* represents the 80%–100% score level with the highest repetitive occurrence rate (mode value) for (N, n), followed by regions in *Green* with lower score levels. The highest mode value of (N, n) (with a score >80%) were (6, 1), (7, 1), (9, 2), (10, 2) for Type-A; (7, 2), (10, 2), (11, 2) for Type-B and (7, 2), (8, 2), (9, 2) for Type-C. Among the obtained (N, n) for each waveform type, the pair with the highest N was used for the performance evaluation of MGD_{WSA} in the validation cohort.

3.2. MGD model-derived flow velocity waveform

A comparison of the MGD-modelled flow velocity waveform ($G_1(t)$) with that of the true flow velocity for various subjects is depicted in figures 5(a), (e), (i). The peaks of $G_1(t)$ and actual flow velocity were coinciding for the validation cohort with an insignificant difference in their temporal sites (0.07 $\pm$ 0.02 s versus 0.06 $\pm$ 0.01 s; $p > 0.05$, respectively). The magnitude spectrum of G_1(i) yielded a -20 dB cut-off within 12–14 Hz, which was also exhibited by the magnitude spectrum of the true flow velocity. The amplitudes of their magnitude spectrum were found to correlate significantly high ($p < 0.001$) with a group average correlation coefficient $r = 0.93 \pm 0.03$, ranged between 0.83 and 0.99 (data not shown).

3.3. Reliability of MGD-modelled pressure and forward–backward wave separation

The RMSE in MGD-modelled pressure waveforms against the true pressure waveforms for Type-A, Type-B, and Type-C were 0.25 $\pm$ 0.10 mmHg, 0.29 $\pm$ 0.11 mmHg, and 0.24 $\pm$ 0.07 mmHg, respectively. The proposed MGD algorithm was able to model the pressure waveform with an RMSE < 0.35 mmHg, which is less than 0.4% of the mean pressure within respective cardiac cycles for the study population.

A sample of the forward–backward components of $P(t)$ constructed using MGD_{WSA} and reference WSA methods for all three types of waveforms are depicted in figures 5(b)–(d), (f)–(h), (j)–(l) for Type-A, B and C respectively. The group average RMSE for P_F(i) obtained from MGD_{WSA} was 1.58 $\pm$ 0.66 mmHg and 1.45 $\pm$ 0.67 mmHg when compared against FD_{WSA} and TD_{WSA}, respectively. For $P_B(t)$, the corresponding RMSEs were 1.56 $\pm$ 0.78 mmHg and 1.41 $\pm$ 0.68 mmHg, respectively.

The pulse pressure of forward wave (ΔP_F) was systematically higher than that of the backward wave (ΔP_B), yielded 23.05 $\pm$ 7.04 mmHg versus 17.75 $\pm$ 5.92 mmHg ($p < 0.001$). Regression analyses of ΔP_F and ΔP_B obtained from MGD_{WSA} against those from the reference WSA methods showed a statistically significant strong

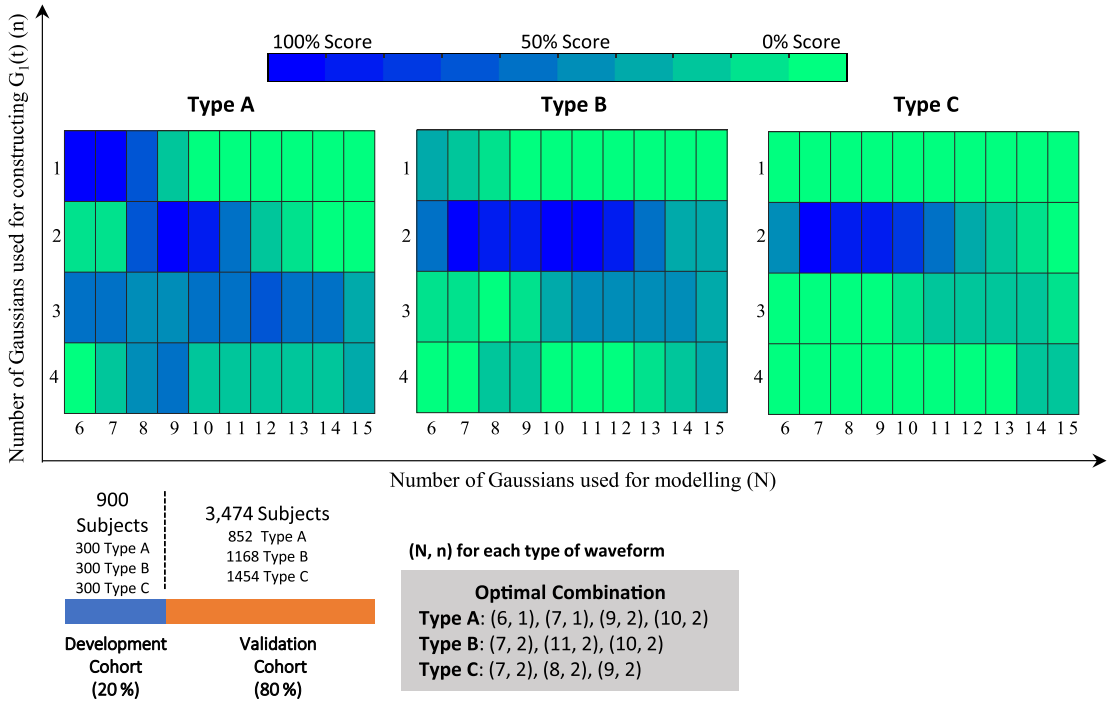

Figure 4. Parametric analysis to obtain the optimal combination of (N, n) using development cohort and their respective score-based heat map.

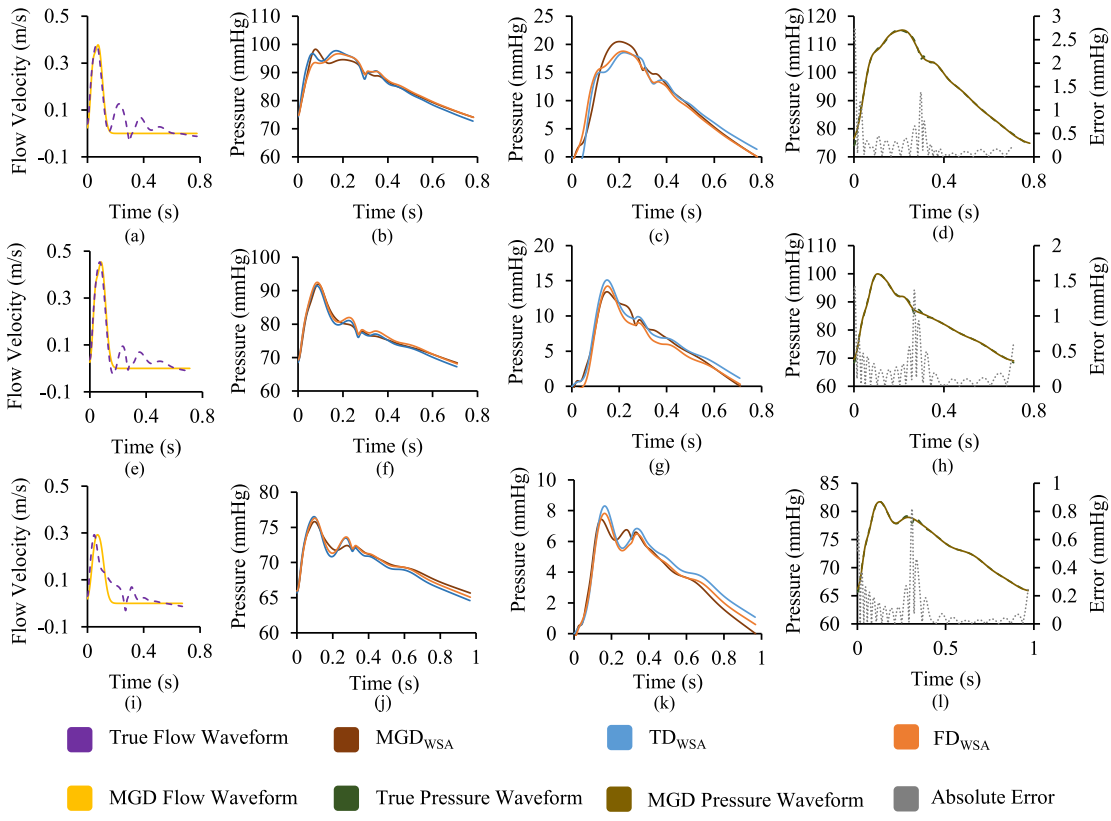

Figure 5. (a), (e), (i) Comparison of true flow velocity waveform and MGD modelled flow velocity, scaled to the peak flow velocity, examples of best-case to worst-case comparison, yielding a deviation in estimated RM from MGD_{WSA} with reference WSA of 0.02, 0.06 and 0.1 respectively. (b)–(d) are forward, backward wave separation, MGD pressure waveform compared with true pressure waveform with the absolute error between them for Type-A subject. (f)–(h) for Type-B and (j)–(k) for Type-C subject.

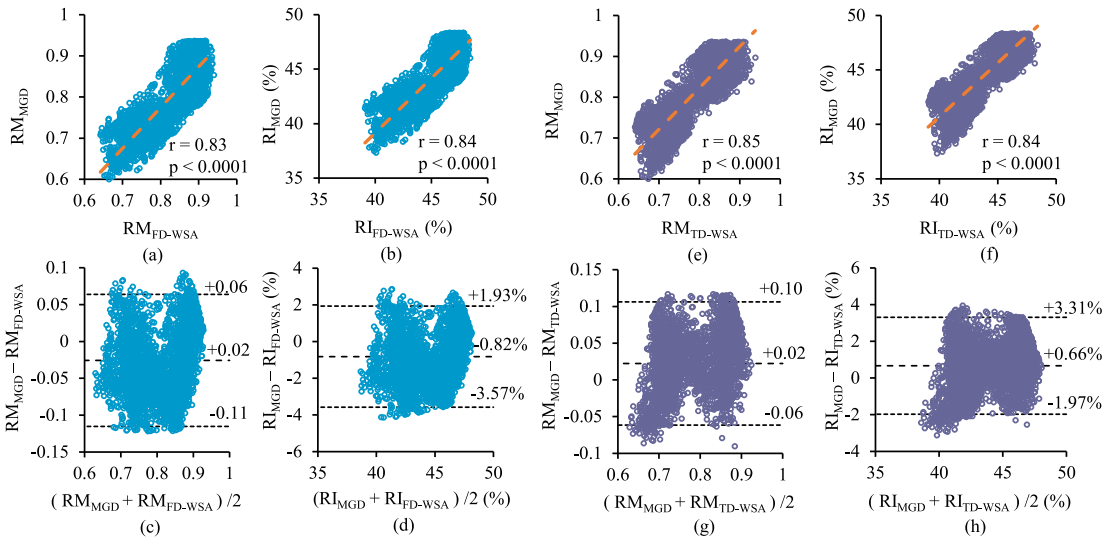

Figure 6. Comparison of reflection parameters (RM and RI) through regression analysis and Bland–Altman plots obtained from MGD_{WSA} and that of FD_{WSA}—(a)–(d), TD_{WSA}—(e)–(h).

correlation ($r > 0.96, p < 0.001$). The deviation in ΔP_F between MGD_{WSA} and FD_{WSA} was 1.81 ± 1.56 mmHg ($p > 0.05$) and was 0.14 ± 1.09 mmHg ($p > 0.05$) against TD_{WSA}. Likewise, the deviation in $MGD_{WSA's}$ ΔP_B against FD_{WSA} and TD_{WSA} were statistically insignificant (1.06 ± 1.22 mmHg ($p > 0.05$) and 0.77 ± 1.04 mmHg ($p > 0.05$), respectively)). Further, BA analyses for ΔP_F and ΔP_B obtained from MGD_{WSA} against FD_{WSA} (Bias = 1.81 mmHg, CI: −1.25 to 4.89 mmHg) for ΔP_F; Bias = 1.06 mmHg (CI: −1.32 to 3.46 mmHg) for ΔP_B) and TD_{WSA} (Bias = 0.14 mmHg, CI: −1.97 to 2.25 mmHg) for ΔP_F; Bias = 0.77 mmHg (CI: −1.27 to 2.81 mmHg) for ΔP_B) revealed no systematic progression of errors.

3.4. Agreement of reflection quantification indices

The group average RM and RI obtained from MGD_{WSA} were 0.79% ± 0.08% and 44.23% ± 2.58%, respectively. The reference WSA methods yielded comparable RM and RI; 0.82% ± 0.07% and 45.05% ± 2.16% for FD_{WSA}, and 0.77% ± 0.07% and 43.56% ± 2.23% for TD_{WSA}. Figure 6 summarizes the regression and BA analyses performed on reflection quantification indices obtained from MGD_{WSA} against those from FD_{WSA} and TD_{WSA} for the validation cohort. Both RM and RI showed a statistically significant strong correlation ($r > 0.83, p < 0.0001$) for MGD_{WSA} versus FD_{WSA} and TD_{WSA} (figures 6(a)–(b), (e)–(f)). The BA analyses for RM and RI obtained from MGD_{WSA} against FD_{WSA} and TD_{WSA} revealed no systematic errors (figures 6(c)–(d), (g)–(h)). The bias for RM and RI between MGD_{WSA} and reference WSA methods was statistically insignificant ($p > 0.05$). Both the reference methods yielded a comparable bias and CI of −0.11 to 0.06, −0.06 to 0.10 for RM and −1.97% to 3.31%, −3.57% to 1.93% for RI, suggesting an acceptable performance of the proposed method.

The group average RWTT was 89 ± 5 ms for MGD_{WSA} , and for the reference WSA methods, RWTT was 83 ± 6 ms, and 88 ± 5 ms for FD_{WSA} and $TD_{WSA,}$ respectively. Regression analysis yielded a statistically significant and strong correlation (r-value $> 0.76, p < 0.001$) for RWTT obtained from MGD_{WSA} with the ones obtained from reference WSA. BA analyses of RWTT compared with both the reference methods had a comparable bias of 0.5 ms, with CI of −5 ms to 6 ms.

4. Discussions

This study was designed to accurately model the pressure waveform using weighted and shifted multi-Gaussians. WSA based on the proposed MGD_{WSA} was performed on the pressure waveforms from the carotid artery, independent of any flow measurements. The performance of the model was estimated by comparing the reflection quantification indices, measured from flow-based reference WSA methods (TD_{WSA} and FD_{WSA}) on 4374 healthy (virtual) subjects. Optimal design parameters (N, n) of MGD_{WSA} for carotid artery are obtained from the development cohort after the parametric analysis. This unique combination of Gaussians (N, n) is used to construct $G_1(t)$ and $G_2(t)$, leading to $P_F(t)$ and $P_B(t)$. The MGD modelled flow velocity waveform ($G_1(t)$) has the majority of the frequency content within the first 15 harmonics; consistent with the theory (Holdsworth *et al* 1999),

about 95–97 percentile of the flow velocity frequency content was within the first 15 harmonics in the frequency domain. For the selected (N, n), the morphology of constructed $G_1(t)$ was found to be an approximation of the $U(t) \times Z_C$ waveform in the systolic phase (refer to figure 5). Since the absolute magnitude of the flow velocity is not required for wave separation (Westerhof *et al* 2006), the obtained $G_1(t)$ was normalized to an arbitrary unit in MGD_{WSA}.

Similar accuracies (RMSE) for forward–backward components of $P(t)$ constructed using MGD_{WSA} ($P_F(t)$ and $P_B(t)$) in the range of 0.82 $\pm$ 0.54 mmHg to 6.66 $\pm$ 4.67 mmHg were reported in the literature for various modelled flow velocity WSA approaches against the reference WSA methods (Westerhof *et al* 2006, Kips *et al* 2009, Hametner *et al* 2013, 2017). The deviations in $P_F(t)$ and $P_B(t)$ (obtained via MGD_{WSA}) from the reference waveforms (obtained via TD_{WSA} and FD_{WSA}) were statistically insignificant ($p > 0.05$), suggesting that the MGD_{WSA} performed a reliable estimation of the forward and backward waves. Prior studies validating WSA techniques have reported deviation in ΔP_F and ΔP_B ranging between -0.01 ± 3.19 mmHg and 5.84 ± 7.18 mmHg (Westerhof *et al* 2006, Kips *et al* 2009, Hametner *et al* 2013, 2017), when compared against the reference method(s) followed herein. Bias and confidence intervals (from BA Analyses) were also on par with those reported in allied studies (Westerhof *et al* 2006, Kips *et al* 2009, Hametner *et al* 2013, 2017). The RWTT, reported prior in the literature, ranges from 40 to 100 ms in Qasem and Avolio (2008), Liu *et al* (2021) and 80 to 180 ms in Segers *et al* (2007). RWTT is often used as a surrogate for carotid-femoral PWV (Qasem and Avolio 2008, Liu *et al* 2021), however, the inaccuracies associated with such approaches need to be further explored (Westerhof and Westerhof 2012).

Therefore, the study results demonstrate the efficiency of the proposed MGD_{WSA} to represent the (modelled) pressure wave and separate it into forward–backward components. Unlike Westerhof *et al* (2006), Kips *et al* (2009), Hametner *et al* (2013, 2017), a notable feature is that the pulse decomposition using MGD model does not involve approximations on the flow velocity waveform. Thus, it provides an opportunity to further explore the decomposition of arterial blood pulse waveforms acquired as plethysmogram (Nabeel *et al* 2017a, 2017b), luminal diameter (Joseph *et al* 2020), or cross-sectional area rather than limiting to pressure waves (Feng and Khir 2010). This allows for reliable biomechanics measurements using techniques such as ultrasound (Pomella *et al* 2017, Nabeel *et al* 2020).

A supplementary analysis was performed to compare the performance of MGD_{WSA} over TF_{WSA}. Reflection quantification indices measured from TF_{WSA} were compared against the reference WSA for the carotid artery, which yielded a moderate correlation ($r \sim 0.50$ to 0.60, $p < 0.0001$) for RM and RI (data not shown). It is evident in the literature that TF_{WSA} is not an appropriate WSA method for non-aortic sites (Kips *et al* 2009, Segers *et al* 2009, Shenouda *et al* 2021). The methodological concerns such as the effect of triangular-shaped approximations and estimated timing of fiducial points (inflection point for flow velocity peak and dicrotic notch for ejection period) were independently studied by Kips *et al* (2009) on 2325 subjects. It concluded that the average flow velocity approximation of aortic flow velocity has a more accurate physiological resemblance than a triangular approximation. Further, Windkessel model-based flow velocity approximation (Hametner *et al* 2013) for aortic flow velocity reported similar accuracy as that of average flow velocity waveform. Though these methods proved to be performing better for aortic flow velocity modelling, the literature lacks evidence of their direct applicability to carotid flow velocity waveforms. Further studies are needed to explore whether aforesaid WSA methods (Qasem and Avolio 2008, Kips *et al* 2009, Swamy *et al* 2010, Hametner *et al* 2013) can be applied to non-aortic sites such as the carotid artery.

There are; however, studies performing non-invasive pressure measurements from the carotid or radial arteries and scale them to aortic sites for WSA. In Qasem and Avolio (2008), Aghilinejad *et al* (2021), Liu *et al* (2021), radial tonometry pulse waves are recorded and scaled to aortic pressure waves based on generalized transfer functions for further WSA based estimations. In Kips *et al* (2009), carotid tonometry pulse waves are used for WSA with flow velocity waveforms recorded from the left ventricular outflow velocity tract.

As alluded to above, aortic WSA is popularly carried out in the literature, which includes approaches that use carotid pressure wave as a surrogate. For instance, at the carotid artery, measuring (or modelling) flow velocity at the same site as that of the pressure measurement has proven advantageous for several clinical applications. Zambanini *et al* (2005) have reported the significance of forward travelling expansion wave, occurring in the mid-systolic region of pressure waves from carotid and peripheral arteries, which is absent in the aortic pulse wave. The majority of cerebral blood flow occurs via the carotid arteries (Chiesa *et al* 2019) have reported the mechanism of cardiovascular pathophysiology leading to cognitive impairment using wave intensity analysis or TF_{WSA}. WSA using simultaneous measurement of pressure/diameter and flow velocity from the carotid artery has opened avenues for monitoring the effect of rapid physiologic perturbations, such as exercise training (Pomella *et al* 2018), lower body negative pressure and cold pressor on carotid artery reactivity, distensibility and change in flow and blood pressure. It has also been employed for the reliable measurement of local pulse wave velocity (Joseph *et al* 2018, Nabeel *et al* 2018b) and central blood pressure (Nabeel *et al* 2018a, 2021, 2022, Raj *et al* 2022).

To the best of our knowledge, the studies that reported WSA using non-invasive pressure and flow velocity from the carotid artery are limited to Niki *et al* (2002), Ohte *et al* (2003), Pomella *et al* (2017), Di Lascio *et al* (2018), Pomella *et al* (2018), using either FD_{WSA} or TD_{WSA}. In this regard, the proposed approach has demonstrated encouraging results by decomposing the carotid pressure waveforms and separating forward–backward components as reliable as the methods based on measuring both the pressure and flow velocity waveforms. Since the carotid artery is a direct branch of the aorta having the anatomical advantage of being a superficial site for non-invasive measurements, the proposed technique has the potential to widen early vascular screening and diagnosis by exploring the carotid biomechanics.

5. Limitations and future scope

Although parametrizing MGD model for various waveform Types (A, B, C) improved the accuracy in estimating reflection quantification indices, a major limiting factor is the sensitivity of the MGD_{WSA} to the waveform morphology and arterial site. For the carotid artery, the Type definitions are well established and can be obtained by examining pressure waveforms in the digital domain. Therefore, the proposed MGD_{WSA} includes waveforms classification as a preliminary step. As of arterial sites are concerned, the model performs better estimation of reflection quantification indices for the ones with a non-substantial retrograde flow (such as the carotid artery) rather than the sites with a significant retrograde flow (such as the radial artery). Gaussian modelling for such flow profiles would involve additional negative Gaussians, which is currently not employed. Improvements in the MGD model developed around retrograde flow profiles are in progress and would potentially be applicable to multiple arterial sites.

A limitation of the study is that the analysis reported herein was performed using a virtual subject dataset. Although it helps to test and deploy the algorithms faster without a human study, an *in vivo* validation is warranted to test the method's usability. This article provides the required theoretical background and a proof of concept on the applicability of the proposed model. An animal study with invasive pressure-flow measures to validate MGD_{WSA} against the reference methods is in progress. Further, a large population cross-sectional study is required to validate the MGD_{WSA}.

6. Conclusion

A WSA method using pressure waveform alone without relying on the actual or modelled flow velocity was developed as an adaptation of the existing wave separation theory. The proposed MGD_{WSA} was validated on a population of healthy (virtual) subjects to demonstrate the proof of concept. The model decomposed the arterial pressure waveform and reliably separated the forward–backward components. The reflection quantification indices (RM, RI, RWTT, ΔP_B, and ΔP_F) obtained from MGD_{WSA} were in agreement with those derived from the reference flow-based WSA methods. The usability of MGD_{WSA} for non-aortic sites having an anatomical advantage such as the carotid artery would widen the scope of early vascular screening and diagnosis using techniques that rely on pulse wave dynamics and non-invasive measurements of plethysmogram, luminal diameter, or cross-sectional area beside the blood pressure waves.

ORCID iDs

Rahul Manoj https://orcid.org/0000-0001-5017-5018
Kiran V Raj https://orcid.org/0000-0003-4078-6856
P M Nabeel https://orcid.org/0000-0001-7280-0048
Jayaraj Joseph https://orcid.org/0000-0002-7279-9099

References

Aghilinejad A, Amlani F, Liu J and Pahlevan N M 2021 Accuracy and applicability of non-invasive evaluation of aortic wave intensity using only pressure waveforms in humans *Physiol. Meas.* **42** 105003

Alastruey J, Parker K H and Sherwin S J 2012 Arterial pulse wave haemodynamics *BHR Gr.—11th Int. Conf. Press Surges* (Lisbon: BHR Group) pp 401–42 (https://kclpure.kcl.ac.uk/portal/files/55965844/Alastruey_et_al_2012_Arterial_pulse_wave_haemodynamics.pdf)

Charlton P H, Harana J M, Vennin S, Li Y, Chowienczyk P and Alastruey J 2019 Modeling arterial pulse waves in healthy aging: a database for in silico evaluation of hemodynamics and pulse wave indexes *Am. J. Physiol.—Heart Circ. Physiol.* **317** H1062–85

Chiesa S T *et al* 2019 Carotid artery wave intensity in mid-to late-life predicts cognitive decline: the Whitehall II study *Eur. Heart J.* **40** 2300–9

Di Lascio N, Gemignani V, Bianchini E, Bruno R M, Ghiadoni L and Faita F 2018 Effects of carotid pressure waveforms on the results of wave separation, wave intensity and reservoir pressure analysis *Physiol. Meas.* **39** 11

Feng J and Khir A W 2010 Determination of wave speed and wave separation in the arteries using diameter and velocity *J. Biomech.* **43** 455–62

Haider A W, Larson M G, Franklin S S and Levy D 2003 Systolic blood pressure, diastolic blood pressure, and pulse pressure as predictors of risk for congestive heart failure in the Framingham heart study *Ann. Intern. Med.* **138** 10–16

Hametner B, Schneider M, Parragh S and Wassertheurer S 2017 Computational assessment of model-based wave separation using a database of virtual subjects *J. Biomech.* **64** 26–31

Hametner B, Wassertheurer S, Kropf J, Mayer C, Holzinger A, Eber B and Weber T 2013 Wave reflection quantification based on pressure waveforms alone-methods, comparison, and clinical covariates *Comput. Methods Prog. Biomed.* **109** 250–9

He Z, Zhang Y, Ma Z, Hu F and Sun Y 2014 A low-pass differentiation filter based on the 2nd-order B-spline wavelet for calculating augmentation index *Med. Eng. Phys.* **36** 786–92

Hoeks A P G, Willigers J M and Reneman R S 2000 Effects of assessment and processing techniques on the shape of arterial pressure-distension loops *J. Vasc. Res.* **37** 494–500

Holdsworth D W, Norley C J D, Frayne R, Steinman D A and Rutt B K 1999 Characterization of common carotid artery blood-flow waveforms in normal human subjects *Physiol. Meas.* **20** 219–40

Hughes A D, Park C, Davies J, Francis D, McG Thom S A, Mayet J and Parker K H 2013 Limitations of augmentation index in the assessment of wave reflection in normotensive healthy individuals *PLoS One* **8** 1–8

Jones C J H and Parker K H 1990 Forward and backward running waves in the arteries: analysis using the method of characteristics *Trans. ASME* **112** 322–6

Joseph J, Kiran R, Nabeel P M, Shah M I, Bhaskar A, Ganesh C, Seshadri S and Sivaprakasam M 2020 ARTSENS® Pen—portable easy-to-use device for carotid stiffness measurement: technology validation and clinical-utility assessment *Biomed. Phys. Eng. Express* **6** 2

Joseph J, Nabeel P M, Shah M I and Sivaprakasam M 2018 Arterial compliance probe for cuffless evaluation of carotid pulse pressure *PLoS One* **13** e0202480

Kips J G, Rietzschel E R, De Buyzere M L, Westerhof B E, Gillebert T C, Van Bortel L M and Segers P 2009 Evaluation of noninvasive methods to assess wave reflection and pulse transit time from the pressure waveform alone *Hypertension* **53** 142–9

Laurent S, Cockcroft J, Van Bortel L, Boutouyrie P, Giannattasio C, Hayoz D, Pannier B, Vlachopoulos C, Wilkinson I and Struijker-Boudier H 2006 Expert consensus document on arterial stiffness: methodological issues and clinical applications *Eur. Heart J.* **27** 2588–605

Liu W, Yao Y, Yang J, Song D, Zhang Y, Sun G, Xu L and Avolio A 2021 Estimation of aortic pulse wave velocity based on waveform decomposition of central aortic pressure waveform *Physiol. Meas.* **42** 105001

London G M, Pannier B and Safar M E 2019 Arterial stiffness gradient, systemic reflection coefficient, and pulsatile pressure wave transmission in essential hypertension *Hypertension* **74** 1366–72

Mynard J P, Kondiboyina A, Kowalski R, Cheung M M H and Smolich J J 2020 Measurement, analysis and interpretation of pressure/flow waves in blood vessels *Front. Physiol.* **11** 1–26

Nabeel P M, Chandran D S, Kaur P, Thanikachalam S, Sivaprakasam M and Joseph J 2021 Association of incremental pulse wave velocity with cardiometabolic risk factors *Sci. Rep.* **11** 1–10

Nabeel P M, Jayaraj J and Mohanasankar S 2017a Single-source PPG-based local pulse wave velocity measurement: a potential cuffless blood pressure estimation technique *Physiol. Meas.* **38** 2122–40

Nabeel P M, Joseph J and Sivaprakasam M 2017b A magnetic plethysmograph probe for local pulse wave velocity measurement *IEEE Trans. Biomed. Circuits Syst.* **11** 1065–76

Nabeel P M, Joseph J, Karthik S, Sivaprakasam M and Chenniappan M 2018a Bi-Modal arterial compliance probe for calibration-free cuffless blood pressure estimation *IEEE Trans. Biomed. Eng.* **65** 2392–404

Nabeel P M, Joseph J and Sivaprakasam M 2018b Variation in local pulse wave velocity over the cardiac cycle: *in vivo* validation using dual-MPG arterial compliance probe *13th Russ. Conf. Biomed. Eng.* pp 100–3

Nabeel P M, Kiran V R, Joseph J, Abhidev V V and Sivaprakasam M 2020 Local pulse wave velocity: theory, methods, advancements, and clinical applications *IEEE Rev. Biomed. Eng.* **13** 74–112

Nabeel P M, Raj V K and Joseph J 2022 Image-free ultrasound for local and regional vascular stiffness assessment: the ARTSENS® Plus *J. Hypertens.* In Press (https://doi.org/10.1097/HJH.0000000000003181)

Nichols W W, O'Rourke M F, Vlachopoulos C, Hoeks A P and Reneman R S 2011 *McDonald's Blood Flow In arteries Theoretical, Experimental and Clinical Principles* 6 (London: CRC Press) 9780429166921 (https://doi.org/10.1201/b13568)

Niki K, Sugawara M, Chang D, Harada A, Okada T, Sakai R, Uchida K, Tanaka R and Mumford C E 2002 A new noninvasive measurement system for wave intensity: evaluation of carotid arterial wave intensity and reproducibility *Heart Vessels* **17** 12–21

Ohte N, Narita H, Sugawara M, Niki K, Okada T, Harada A, Hayano J and Kimura G 2003 Clinical usefulness of carotid arterial wave intensity in assessing left ventricular systolic and early diastolic performance *Heart Vessels* **18** 107–11

Papaioannou T G, Stamatelopoulos K S, Gialafos E, Vlachopoulos C, Karatzis E, Nanas J and Lekakis J 2004 Monitoring of arterial stiffness indices by applanation tonometry and pulse wave analysis: reproducibility at low blood pressures *J. Clin. Monit. Comput.* **18** 137–44

Pomella N, Wilhelm E N, Kolyva C, González-Alonso J, Rakobowchuk M and Khir A W 2017 Common carotid artery diameter, blood flow velocity and wave intensity responses at rest and during exercise in young healthy humans: a reproducibility study *Ultrasound Med. Biol.* **43** 943–57

Pomella N, Wilhelm E N, Kolyva C, González-Alonso J, Rakobowchuk M and Khir A W 2018 Noninvasive assessment of the common carotid artery hemodynamics with increasing exercise work rate using wave intensity analysis *Am. J. Physiol.—Hear. Circ. Physiol.* **315** H233–41

Qasem A and Avolio A 2008 Determination of aortic pulse wave velocity from waveform decomposition of the central aortic pressure pulse *Hypertension* **51** 188–95

Qureshi M U, Colebank M J, Schreier D A, Tabima D M, Haider M A, Chesler N C and Olufsen M S 2018 Characteristic impedance: frequency or time domain approach? *Physiol. Meas.* **39** 1

Raj K V, Nabeel P M, Chandran D, Sivaprakasam M and Joseph J 2022 High-frame-rate a-mode ultrasound for calibration-free cuffless carotid pressure: feasibility study using lower body negative pressure intervention *Blood Press* **31** 19–30

Segers P *et al* 2017 *Towards a Consensus on the Understanding and Analysis of the Pulse Waveform: Results from the 2016 Workshop on Arterial Hemodynamics: Past, Present and Future* 18, pp. 75–80

Segers P, Kips J, Trachet B, Swillens A, Vermeersch S, Mahieu D, Rietzschel E, De Buyzere M and Van Bortel L 2009 Limitations and pitfalls of non-invasive measurement of arterial pressure wave reflections and pulse wave velocity *Artery Res.* **3** 79–88

Segers P, Rietzschel E R, De Buyzere M L, De Bacquer D, Van Bortel L M, De Backer G, Gillebert T C and Verdonck P R 2007 Assessment of pressure wave reflection: getting the timing right! *Physiol. Meas.* **28** 1045–56

Shenouda N, Stock J M, Patik J C, Chirinos J A and Edwards D G 2021 Personalized physiologic flow waveforms improve wave reflection estimates compared to triangular flow waveforms in adults *Am. J. Physiol.—Hear. Circ. Physiol.* **320** H1802–12

Swamy G, Olivier N B and Mukkamala R 2010 Calculation of forward and backward arterial waves by analysis of two pressure waveforms *IEEE Trans. Biomed. Eng.* **57** 2833–39

Swillens A and Segers P 2008 Assessment of arterial pressure wave reflection: methodological considerations *Artery Res.* **2** 122–31

Takazawa K, Tanaka N, Takeda K, Kurosu F and Ibukiyama C 1995 Underestimation of vasodilator effects of nitroglycerin by upper limb blood pressure *Hypertension* **26** 520–3

Tomiyama H, O'Rourke M F, Hashimoto H, Matsumoto C, Odaira M, Yoshida M, Shiina K, Nagata M and Yamashina A 2013 Central blood pressure: a powerful predictor of the development of hypertension *Hypertens. Res.* **36** 19–24

van den Wijngaard J P H M, Siebes M and Westerhof B E 2009 Comparison of arterial waves derived by classical wave separation and wave intensity analysis in a model of aortic coarctation *Med. Biol. Eng. Comput.* **47** 211–20

Wang L, Xu L, Feng S, Meng M Q H and Wang K 2013 Multi-Gaussian fitting for pulse waveform using weighted least squares and multi-criteria decision making method *Comput. Biol. Med.* **43** 1661–72

Westerhof B E, Guelen I, Westerhof N, Karemaker J M and Avolio A 2006 Quantification of wave reflection in the human aorta from pressure alone: a proof of principle *Hypertension* **48** 595–601

Westerhof B E and Westerhof N 2012 Magnitude and return time of the reflected wave: the effects of large artery stiffness and aortic geometry *J. Hypertens.* **30** 93932–39

Westerhof N, Segers P and Westerhof B E 2015 Wave separation, wave intensity, the reservoir-wave concept, and the instantaneous wave-free ratio: presumptions and principles *Hypertension* **66** 93–98

Westerhof N, Sipkema P, Den Bos G C V and Elzinga G 1972 Forward and backward waves in the arterial system *Cardiovasc. Res.* **6** 648–56

Wilkinson I B, Fuchs S A, Jansen I M, Spratt J C, Murray G D, Cockcroft J R and Webb D J 1998 Reproducibility of pulse wave velocity and augmentation index measured by pulse wave analysis *J. Hypertens.* **16** 2079–84

Zambanini A, Cunningham S L, Parker K H, Khir A W, Thom S A M G and Hughes A D 2005 Wave-energy patterns in carotid, brachial, and radial arteries: a noninvasive approach using wave-intensity analysis *Am. J. Physiol.—Hear. Circ. Physiol.* **289** 270–6